The Evolution of Volatile Production in comet C/2009 P1 (Garradd) During its 2011-2012 Apparition.

A. Gicquel [1,2], S. N. Milam [1], I. M. Coulson [3], G. L. Villanueva [1,2], M. A. Cordiner [1,2], S. B. Charnley [2], M. A. DiSanti [2], M. J. Mumma [2] and S. Szutowicz [4]

ABSTRACT

We report observations at millimeter and submillimeter wavelengths of comet C/2009 P1 (Garradd) from 2011 December 28 to 2012 April 24, using the Arizona Radio Observatory submillimeter telescope (SMT) and the James Clerk Maxwell Telescope (JCMT). Garradd is a dynamically young long-period comet from the Oort Cloud, with a periodicity of 127,000 years, that reached perihelion on 2011 December 23 (at R_h = 1.55 AU and Δ = 20.1 AU) and made its closest approach to the Earth on 2012 March 05 (at R_h = 1.84 AU and Δ = 1.26 AU). We obtained gas production rates, and molecular abundances relative to water for HCN, *ortho*-H_2CO, CS, CO and CH_3OH. A rotational temperature, $T_{rot} \approx 50$ K, was determined by observing multiple methanol lines with the JCMT. By averaging the abundance ratio relative to water from the SMT and the JCMT we derive: CO: 7.03 ± 1.84 %, HCN: 0.04 ± 0.01 %, o-H_2CO: 0.14 ± 0.03 % as a parent molecule (and 0.28 ± 0.06 % as an extended source), CS: 0.03 ± 0.01 % and CH_3OH: $3.11^{+1.86}_{-0.51}$ %. We concluded that Garradd is normal in CH_3OH, depleted in HCN, o-H_2CO and CS and slightly enriched in CO with respect to typically observed cometary mixing ratios. We also studied the temporal evolution of HCN and CO and find that the production of HCN has a trend similar to water (but with short-term variation), with a decrease after perihelion, while that of CO shows contrary behavior: remaining constant or increasing after perihelion.

Subject headings: Astrobiology – Solar System: general – Comets: individual (C/2009 P1 (Garradd)) – techniques: spectroscopic – submm lines: Solar System

---

[1]Catholic University of America, Physics Department, 620 Michigan ave NE, Washington, DC;

[2]Goddard Center for Astrobiology, NASA Goddard Space Flight Center, 8800 Greenbelt Rd., Greenbelt, MD 20771, USA; adeline.gicquel@nasa.gov, stefanie.n.milam@nasa.gov, geronimo.villanueva@nasa.gov, martin.a.cordiner@nasa.gov, steven.b.charnley@nasa.gov, michael.a.disanti@nasa.gov, michael.j.mumma@nasa.gov

[3]Joint Astronomy Centre, 660 N. A'ohoku Place University Park, Hilo, Hawaii 96720, USA; i.coulson@jach.hawaii.edu

[4]Space Research Centre PAS, Str. Bartycka 18A, 00-716 Warsaw, Poland; slawka@cbk.waw.pl

1. Introduction

Comets are among the most pristine objects in our Solar System. Their chemical composition provides important clues to the processes that occurred during the formation and early evolution of the Solar System. Cometary nuclei today reside in (at least) two distinct reservoirs, the Oort Cloud (OC) and the Edgeworth-Kuiper Belt (EKB) (divided into the classical KB, the scattered disk, and the detached or extended disk populations; Morbidelli et al. (2008)). Once injected into the inner planetary system, comets are classified dynamically as nearly isotropic [long-period comet (LPC) or Halley-type comet (HTC)] or ecliptic [Centaur-type, Encke-type, or Jupiter-family comet (JFC)]. The Tisserand parameter of the current orbit of a given comet identifies the storage reservoir from whence it came; ecliptic comets come from the scattered KB reservoir, whereas the storage reservoir for nearly isotropic comets (NICs) is the OC (Levison et al. 1996; Horner et al. 2003). Past observations have shown that comets appear to contain a mixture of products from both interstellar and nebular chemistries and could also have been important for initiating prebiotic chemistry on the early Earth (Ehrenfreund & Charnley 2000). Although there are some differences, the volatile composition of cometary ices is generally similar to the inventory of molecules detected in the ices and gas of dense molecular clouds. Given the gradient in physical conditions expected across the proto-Solar nebula, chemical diversity in the comet population is to be expected, as has been inferred for both JFCs (Crovisier et al. 2009; Gicquel et al. 2014) and OCs comets (DiSanti & Mumma 2008).

Comet C/2009 P1 (Garradd), hereafter Garradd, was discovered on 2009 August 13 at a heliocentric distance $R_h = 8.7$ AU (McNaught & Garradd 2009). The comet reached perihelion on 2011 December 23 at $R_h = 1.55$ AU and perigee at $\Delta = 1.27$ AU on 2012 March 05. Observations were made throughout this period by many groups using both ground-based and space-based telescopes (e.g., Paganini et al. (2012), Bodewits et al. (2014) and Villanueva et al. (2012)). Based on the inclination to the ecliptic, Tisserand parameter, and original semi-major axis, comet Garradd can be classified as a probable dynamically young, long period comet from the Oort Cloud, whereas a classification based on its activity is less definitive, due to the diversity in composition both among and within the different comet populations.

New dynamically young comets from the Oort Cloud (on their first trip back to the inner Solar System) may reveal primordial composition while the composition of comets in short orbits may be altered with each passage. Also, probably due to a different composition or the effect of the Solar heating (Oort & Schmidt 1951; A'Hearn et al. 1995; Cordiner et al. 2014; Combi et al. 2014), dynamically new comets (like ISON) have shown different behavior. However, they tend to be more active during their early approach to the Sun and develop

more normal activity later in the apparition (Meech & Svoren 2004; Meech et al. 2009).

Garradd's pre-perihelion peak in water production between 100 - 50 days before perihelion (Combi et al. 2013; Bodewits et al. 2014) and monotonically increase of CO activity post-perihelion (Feaga et al. 2014) is in contrast with the behaviour of the well studied Oort-Cloud comet C/1995 O1 (Hale-Bopp), which showed an increase of all gas production rates pre-perihelion and a decrease afterwards (Biver et al. 2002). Garradd has also been defined as CO-rich, having a abundance ratio of CO relative to water between 9.12 ± 0.80 and 13.45 ± 1.45 % (Paganini et al. 2012; Villanueva et al. 2012; DiSanti et al. 2014), which is consistent with other active Oort Cloud comets like C/1995 O1 (Hale-Bopp) and C/1996 B2 (Hyakutake).

Intriguing early observations of comet Garradd, presented an opportunity to expand the still small database of observations of comets, from which eventually will emerge an understanding of their formation, evolution, and perhaps taxonomy.

We conducted observations at submillimeter wavelengths of comet Garradd from 2011 December 28 to 2012 April 24. Here we report detections of HCN, o-H_2CO, CS, CO and CH_3OH using the Arizona Radio Observatory submillimeter telescope (SMT) and the James Clerk Maxwell Telescope (JCMT). We present the observational results and determine physical parameters such as rotational temperature, column densities, production rates, and abundance ratios.

2. Observations

All the observations presented here were obtained using the JPL/Horizons (Jet Propulsion Laboratory) ephemeris number 82.

2.1. Arizona Radio Observatory Submillimeter Telescope (SMT)

Observations of HCN:J=3-2 (265.8864 GHz), CO:J=2-1 (230.5380 GHz), CS:J=5-4 (244.9356 GHz), o-H_2CO:J_{K_a,K_c}=$3_{1,2}$-$2_{1,1}$ (225.6978 GHz), and CH_3OH:J=5-4, toward comet C/2009 P1 (Garradd) were conducted between 2011 December 28 and 2012 March 06 using the 10m Arizona Radio Observatory Submillimeter Telescope (SMT) on Mount Graham, Arizona. These data were obtained with a dual-polarization ALMA Band 6 receiver system, employing sideband-separating mixers with an image rejection of typically 14–25 dB. The backends employed were a 2048 channel 1 MHz and 250 kHz filter banks used in parallel mode. The temperature scale at the SMT is T_A^*; radiation temperature is then defined as

$T_R = T_A^*/\eta_b$, where η_b is the main beam efficiency. Data were taken in position-switching mode with an off position 30' west in azimuth. The pointing accuracy is estimated at 1" rms. Focus and positional accuracy were checked periodically on nearby planets and masers.

2.2.   James Clerk Maxwell Telescope (JCMT)

Observations of C/2009 P1 (Garradd) were made from the JCMT, located at the 4000m level on Mauna Kea, Hawaii, on multiple occasions from 2011 December 30 to 2012 April 24, using the HARP heterodyne array in single-receptor mode. For this work, HARP was tuned for the transitions of HCN:J=4-3 (354.5055GHz) and CO:J=3-2 (345.7986GHz), employing the ACSIS digital correlation spectrometer configured at its highest frequency resolution (31 kHz), and subsequently smoothed prior to presentation here.

At these frequencies, the JCMT has a Gaussian beam of size $\approx$ 15" (full width at half power). Pointing of the telescope was verified approximately every hour and was achieved by doing spectral-line 'five-points' on nearby line sources. The pointing accuracy is estimated at 2" rms in each of two orthogonal coordinates (azimuth and elevation). Telescope focus is similarly maintained throughout the night by measures of bright line-sources. Calibration of the (T_A^*) brightness scale is achieved by making measures at standard frequencies (e.g. CO:J=3-2, 345GHz) of astronomical sources used as reference calibrators. As for the SMT, the radiation temperature is defined as $T_R = T_A^*/\eta_b$.

The opacity of the sky above JCMT was measured by a water vapor meter (WVM) mounted so as to measure along the telescope line-of-sight. Opacity is expressed as if measured at the zenith at 225GHz. The opacity (in nepers) on UT 2011 December 30, 2012 January 20 and 22, February 29, March 26, and April 24, was on average, 0.05, 0.10, 0.06, 0.14, 0.18, 0.07, respectively. Spectroscopic data were reduced using STARLINK software *smurf/makecube* and analyzed using *kappa/splat*.

3.   Results

Circumstances of the observations - UT date, observing frequency (ν), beam size (Θ_b), diameter of the projected beam size on the comet (D), main beam efficiency (η_b), heliocentric distance (R_h) and comet distance at the times of measurements (Δ) - are listed in Table1. The integrated line intensity ($\int T_A^* \, d_v$) derived from a Gaussian fit and the associated 1σ uncertainty are also given in Table.1.

Representative spectra from both facilities are shown in Figure 1, plotted in a come-

Table 1.   Observations HCN, CO, CS, o-H$_2$CO and CH$_3$OH toward comet C/2009 P1 (Garradd) from SMT and JCMT.

Line	Telescope	Transition	UT Date	Figure Reference	ν (MHz)	Θ_b (")	D (km)	η_b	$\int T_A^* \, d_v$ km s^{-1}	R$_h$ (AU)	Δ (AU)
HCN	SMT	3-2	2011 Dec 28.94	a	265886.4	28.4	40568	0.74	0.32 ± 0.02	1.55	1.97
			2011 Dec 29.33	b			40465		0.26 ± 0.02	1.55	1.96
			2012 Jan 18.52	c			35008		0.30 ± 0.02	1.59	1.74
			2012 Jan 19.53	d			35481		0.35 ± 0.02	1.59	1.72
			2012 Feb 18.46	e			27739		0.17 ± 0.01	1.73	1.35
			2012 Feb 19.36	f			27553		0.31 ± 0.02	1.74	1.34
			2012 Feb 23.62	g			26894		0.26 ± 0.01	1.76	1.31
			2012 Mar 06.32	h			26070		0.28 ± 0.02	1.84	1.27
CO	SMT	2-1	2012 Jan 18.63	i	230238.0	32.7	41231		0.04 ± 0.01	1.59	1.74
			2012 Feb 18.60	j			31992		0.04 ± 0.01	1.73	1.35
			2012 Mar 06.55	k			30068		0.04 ± 0.01	1.84	1.27
CS	SMT	5-4	2012 Mar 06.55	l	244935.6	30.8	30111		0.04 ± 0.01	1.73	1.35
o-H$_2$CO		$3_{1,2} - 2_{1,1}$	2012 Feb 19.70	m	225697.8	33.4	32459		0.03 ± 0.01	1.74	1.34
			2012 Mar 06.67	n			30712		0.03 ± 0.01	1.84	1.27
CH$_3$OH	SMT	5-4	2012 Feb 19.46	o	241700.2	31.2	30310		0.08 ± 0.02	1.74	1.34
					241767.2		30302		0.08 ± 0.01		
					241791.4		30300		0.09 ± 0.01		
					241904.2		30285		0.04 ± 0.01		
					241904.6		30285		0.04 ± 0.01		
			2012 Mar 06.46	p	241700.2		28679		0.06 ± 0.02	1.84	1.27
					241767.2		28671		0.08 ± 0.01		
					241791.4		28668		0.08 ± 0.01		
					241879.1		28658		0.04 ± 0.01		
					241904.1		28655		0.06 ± 0.02		
					241904.6		28655		0.06 ± 0.02		
CO	JCMT	3-2	2011 Dec 30.74	q	345796.0	14.6	20584	0.63	0.13 ± 0.03	1.55	1.95
			2012 Jan 20.84	r			17945		0.13 ± 0.03	1.60	1.70
			2012 Jan 22.85	s			17628		0.13 ± 0.04	1.61	1.67
			2012 Feb 29.60	t			13406		0.20 ± 0.05	1.81	1.27
			2012 Mar 26.29	u			15095		0.16 ± 0.05	2.00	1.43
HCN	JCMT	4-3	2012 Jan 22.82	v	354505.5	14.2	17195		0.24 ± 0.03	1.61	1.67
			2012 Mar 26.34	w			14724		0.26 ± 0.08	2.00	1.43
			2012 Apr 24.27	x			20799		0.09 ± 0.02	2.25	2.02

tocentric velocity frame, and labelled by a letter corresponding to the entries in Table 1. Figure 1 shows the CO:J=3-2 and HCN:J=4-3 transitions observed from comet Garradd on 2012 March 26 from JCMT, and the CO:J=2-1, HCN:J=3-2, CS:J=5-4 and o-H$_2$CO:J$_{K_a,K_c}$=$3_{1,2} - 2_{1,1}$ transitions observed on 2012 March 06 from the SMT. Gas production rates from these transitions are reported in Table 2. Figure 2 shows the spectra of CH$_3$OH:J=5-4 taken on 2012 February 19, and March 26 with the SMT. Derivation of the rotational temperature of CH$_3$OH can be found in section 4.1, the computation of the column densities, production rates and abundances ratios is in section 4.2, and a detailed discussion about the temporal evolution of water, CO and HCN is in section 4.3. All data are available in the online journal as supplemental information.
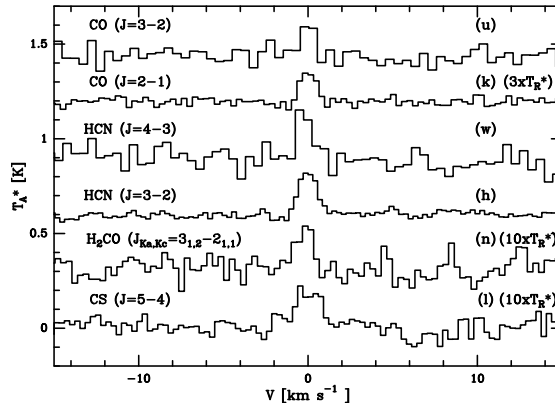

Fig. 1.— Detection of CO (J=3-2), CO (J=2-1), HCN (J=4-3), and HCN (J=3-2), o-H$_2$CO (J_{K_a,K_c}=$3_{1,2} - 2_{1,1}$), and CS (J=5-4) taken on 2012 March 06 (k, h, n and l) and March 26 (u and w) with the JCMT and the SMT. See Table 1 for dates, parameters of observations, and reference letters on the right-hand side of each panel. **Additional spectra for the observing campaign for CO, HCN and o-H$_2$CO are available in the online journal. Note that the plots n, h, w, k and u are offset from the baseline at zero.**

4. Analysis

4.1. Rotational temperature

We have applied the rotational diagram technique (Schloerb et al. 1983; Blake et al. 1986; Bockelée-Morvan et al. 1994; Drahus et al. 2012) to our SMT methanol data to determine the coma temperature and the total number of methanol molecules observed in the beam. We assume local-thermodynamic-equilibrium (LTE), thus a linear ln(F)=f(E$_u$) provides the

temperature and the column density:

$$ln\left(\frac{N_u}{g_u}\right) = ln\left(\frac{N_{tot}}{\zeta_{rot}}\right) - \frac{E_{up}}{kT_{rot}} \qquad (1)$$

with :

$$N_u = \frac{8\pi k \nu^2 \int T_A^* \Delta v_{1/2}}{hc^3 A_{ul} \eta_b} \qquad (2)$$

where N_u [cm^{-2}] is column density upper energy level, k is the Boltzmann constant, ζ_{rot} is the partition function, h is the Planck constant, c is the speed of the light, A_{ul} [s^{-1}] is the Einstein coefficient, g_{up} is the statistical weight, T_{rot} [K] is the rotational excitation temperature, E_{up} [cm^{-1}] is the upper state energy, and N_{tot} [cm^{-2}] is the total number of molecules observed in the beam. We observed methanol lines on 2012 February 19 (R_h =1.74 AU) and March 06 ($R_h = 1.84$ AU) with the SMT, see Figure 2. The intensities of the five and six observed methanol lines (Figure 2), allowed us to determine a poorly constrain rotational temperature $T_{rot} = 46^{+32}_{-13}$ K (2012 Feb. 19) and $T_{rot} = 46^{+33}_{-14}$ K (2012 March 06), or $T_{rot} \approx 50$ K. Our value is in good agreement with Biver et al. (2012), who derived an average of the gas temperature in the coma of $\sim$50 K from observations of 70 lines of methanol obtained with the IRAM-30m telescope on 2011 October and 2012 February. Using JCMT data taken on 2012 July 28-31 and January 06-08, Yang & Drahus (2012) showed that T_{rot} varied with R_h, going from $T_{rot} \approx 30$ K at $R_h = 2.49$ AU, to $T_{rot} \approx 40$ K at $R_h = 1.56$ AU. From the HCN lines observed on 2011 September 8 and 9 using the high-resolution infrared spectrometers (NIRSPEC at Keck II and CHSELL at IRTF), Villanueva et al. (2012) determined $T_{rot} = 40 \pm 7$ K (R_h = **2.1 AU**). Also from infrared data (CRIRES at ESO's Very Large Telescope), Paganini et al. (2012) concluded that a $T_{rot} \approx 50$ K is consistent with the average temperature from the volatiles of H$_2$O, CO, C$_2$H$_6$, HCN, and CH$_3$OH on 2011 September 17-21 ($R_h = 2.00$ AU). Finally, on 2011 October 13 ($R_h = 2.00$ AU), DiSanti et al. (2014) obtained a (poorly constrained) rotational temperature for water $T_{rot} = 42^{+26}_{-24}$ K.

Also the column densities for CH$_3$OH, have been derived from the rotational diagram and are listed in Table 2.

4.2.   Column densities, Production rates and Abundances ratios

Beam-averaged column densities were derived for CO, HCN, CS and o-H$_2$CO assuming that the cometary coma filled the beams of the respective telescopes. The column densities for the observations were calculated using equation 2 from Gicquel et al. (2014) with $T_{rot} =$ 50 K. The column densities derived for CO, HCN, CS and o-H$_2$CO are listed in Table 2.
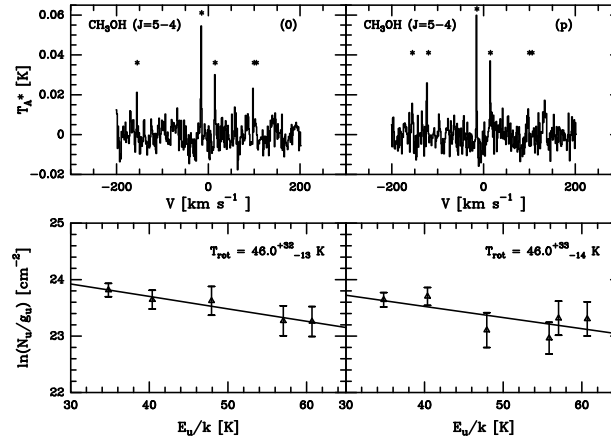
Fig. 2.— Detection of CH$_3$OH (J=5-4) taken on 2012 February 19 (o), and March 26 (p) with the SMT and rotational diagram. See Table 1 for dates, parameters of observations, and reference letters on the right-hand side of each panel. (*) denote CH$_3$OH lines.

The production rates were derived for CO, HCN, CS and o-H$_2$CO from a Monte Carlo model described in Milam et al. (2004, 2006). **CO and HCN, are calculated as parent molecules. CS is considered as both a parent and a daughter species. o-H$_2$CO is calculated as both a parent and an extended source species.** In the case of CO, HCN, CS and o-H$_2$CO as parents molecules, we used the velocity law $v_p = 0.8R_h^{-0.5}$ [kms^{-1}] from Biver et al. (1999). **The determination of the velocity from the CO, CS and o-H$_2$CO lines are difficult so the integrated line intensity is derived directly from a Gaussian fit (e.g. section 3). To confirm the hypothesis of the above law, we derived velocity FHWM from fits of the HCN lines. The velocity derived from the observations are in good agreement with the velocity law. To conclude, for simplification and coherence in the analysis we adopt v_p defined above for all observations.** For o-H$_2$CO as an extended source, we used parent scale lengths in the range $(4000\text{-}8000)R_h^{1.5}$ [km] (after Biver et al. (1999)) and a velocity law equal to $v_p = 0.6R_h^{-0.25}$ [km s^{-1}] for the parent species (Combi & Fink 1997; Milam et al. 2006) and $v_d = 0.8R_h^{-0.5}$ [kms^{-1}] for the daughters molecules. From the first observations of comets with ALMA, Cordiner et al. (2014) found smaller scale lengths (a few thousand kilometers in comet Lemmon (at R$_h$ = 1.5 AU) and only a few hundred kilometers in comet ISON (at R$_h$ = 0.45 AU) probing only the innermost few thousand km of the coma. Our observations have distances up to ≈ 20,000 km from the nucleus, so the scale lengths of Biver et al. (1999), derived from single dish observations, are more applicable for these data. **For CS as a daughter molecule, we assumed a production from a short-lived species such as CS$_2$ (Snyder et al.**

2001) with a lifetime equal $370R_h^2$ [s] (Huebner et al. 1992). CS_2 has much smaller photo-dissociation scale length ($\approx$ 300 km) than the beam radius (1.5×10^4 km), so the difference between the gas production of CS as daughter molecule or as a parent molecule is negligible (DiSanti et al. 2009).

Table 2 summarizes the production rates of the molecules observed toward comet C/2009 P1 (Garradd). This model assumes isotropic outgassing, which is reasonable for the analysis of these data since the model simulates the observed column densities within a large beam (with respect to the comet). The uncertainties introduced into the modeled production rates are dominated by the errors on the measured column densities. We used the production rate of water from Combi et al. (2013), Feaga et al. (2014) (on 2012 March 26), Bockelée-Morvan et al. (2014) (on 2012 February 17 and 23) and Bodewits et al. (2014) (on 2012 April 24) to obtain the Q/Q_{H_2O} ratio with the SMT and JCMT.

Combi et al. (2013) observed water every 2 days on average from 2011 August 15 to 2012 April 6 with SWAN (Solar Wind Anisotropies). Also, Bodewits et al. (2014) acquired 107 observations from 2011 April to 2012 October with $Swift$/UVOT. They both identified an asymmetry of Q_{H_2O} about perihelion, with larger values before perihelion than after and different trends with heliocentric distance. The gas production rate of water peaks around 50 - 100 days before the perihelion (Figure 3). **In this figure, we used the curve from Bodewits et al. (2014) to give an idea of the temporal production rate of water by averaging data in IR, mm-sub and UV.** These results highlight the importance of using the Q_{H_2O} at the same date as our observations if the correct abundance ratio is to be determined for comparisons to other targets and dates.

Table 2. Beam average column densities, photodissociation rates, production rates of HCN, CO, CS, o-H$_2$CO and CH$_3$OH, production rates of water and the ratio Q/Q_{H_2O} with the SMT and JCMT.

Line	Telescope	Transition	UT Date	N_{tot} (cm^{-2})	Rate[a] (s^{-1})	Q (s^{-1})	Q_{H_2O}[b] (s^{-1})	Q/Q_{H_2O} (%)
HCN	SMT	3-2	2011 Dec 28.99	$(3.81 \pm 0.24) \times 10^{11}$	1.31×10^{-05}	$(1.22 \pm 0.08) \times 10^{26}$	$(1.93 \pm 0.08) \times 10^{29}$	$(6.32 \pm 0.47) \times 10^{-2}$
			2011 Dec 29.33	$(3.11 \pm 0.29) \times 10^{11}$		$(9.83 \pm 0.09) \times 10^{25}$	$(1.93 \pm 0.08) \times 10^{29}$	$(5.09 \pm 0.51) \times 10^{-2}$
			2012 Jan 18.52	$(3.62 \pm 0.25) \times 10^{11}$		$(9.48 \pm 0.66) \times 10^{25}$	$(2.33 \pm 0.03) \times 10^{29}$	$(4.07 \pm 0.29) \times 10^{-2}$
			2012 Jan 19.53	$(4.21 \pm 0.24) \times 10^{11}$		$(1.12 \pm 0.06) \times 10^{26}$	$(2.33 \pm 0.03) \times 10^{29}$	$(4.81 \pm 0.28) \times 10^{-2}$
			2012 Feb 18.46	$(2.01 \pm 0.11) \times 10^{11}$		$(3.87 \pm 0.22) \times 10^{25}$	$(1.20 \pm 0.03) \times 10^{29}$	$(3.23 \pm 0.20) \times 10^{-2}$
							$(1.10 \pm 0.03) \times 10^{29c}$	$(3.52 \pm 0.22) \times 10^{-2}$
			2012 Feb 19.36	$(3.69 \pm 0.19) \times 10^{11}$		$(7.04 \pm 0.36) \times 10^{25}$	$(1.04 \pm 0.07) \times 10^{29}$	$(6.77 \pm 0.57) \times 10^{-2}$
			2012 Feb 23.62	$(3.09 \pm 0.20) \times 10^{11}$		$(5.65 \pm 0.22) \times 10^{25}$	$(9.38 \pm 0.27) \times 10^{28}$	$(6.02 \pm 0.29) \times 10^{-2}$
							$(0.75 \pm 0.05) \times 10^{29c}$	$(7.53 \pm 0.50) \times 10^{-2}$
CO		2-1	2012 Mar 06.32	$(3.37 \pm 0.23) \times 10^{11}$	7.49×10^{-07}	$(5.89 \pm 0.39) \times 10^{25}$	$(9.50 \pm 0.70) \times 10^{28}$	$(6.20 \pm 0.62) \times 10^{-2}$
			2012 Jan 18.63	$(4.02 \pm 0.84) \times 10^{13}$		$(1.08 \pm 0.23) \times 10^{28}$	$(2.33 \pm 0.03) \times 10^{29}$	4.64 ± 0.97
			2012 Feb 18.60	$(3.43 \pm 0.85) \times 10^{13}$		$(6.82 \pm 1.69) \times 10^{27}$	$(1.20 \pm 0.03) \times 10^{29}$	5.69 ± 1.42
							$(1.10 \pm 0.03) \times 10^{29c}$	6.20 ± 1.55
CS		5-4	2012 Mar 06.55	$(3.43 \pm 0.86) \times 10^{13}$	1.00×10^{-05}	$(6.20 \pm 1.56) \times 10^{27}$	$(9.50 \pm 0.70) \times 10^{28}$	6.53 ± 1.71
			2012 Feb 18.85	$(1.67 \pm 0.21) \times 10^{11}$		$(3.40 \pm 0.46) \times 10^{25}$	$(1.20 \pm 0.03) \times 10^{29}$	$(2.84 \pm 0.39) \times 10^{-2}$
							$(1.10 \pm 0.03) \times 10^{29c}$	$(3.09 \pm 0.43) \times 10^{-2}$
o-H$_2$CO		$3_{1,2} - 2_{1,1}$	2012 Feb 19.70	$(2.27 \pm 0.38) \times 10^{11}$	2.15×10^{-04}	$(1.49 \pm 0.25) \times 10^{26d}$	$(1.04 \pm 0.06) \times 10^{29}$	$(1.44 \pm 0.26) \times 10^{-1d}$
					1.73×10^{-04e}	$(2.41 \pm 0.40) \times 10^{26e}$		$(2.33 \pm 0.41) \times 10^{-1e}$
					8.65×10^{-05f}	$(3.43 \pm 0.57) \times 10^{26f}$		$(3.31 \pm 0.59) \times 10^{-1f}$
			2012 Mar 06.67	$(2.36 \pm 0.63) \times 10^{11}$	2.15×10^{-04}	$(1.28 \pm 0.35) \times 10^{26d}$	$(9.50 \pm 0.70) \times 10^{28}$	$(1.35 \pm 0.38) \times 10^{-1d}$
					1.73×10^{-04e}	$(2.08 \pm 0.57) \times 10^{26e}$		$(2.19 \pm 0.61) \times 10^{-1e}$
					8.65×10^{-05f}	$(3.02 \pm 0.81) \times 10^{26f}$		$(3.18 \pm 0.88) \times 10^{-1f}$
CH$_3$OH		5-4	2012 Feb 19.46	$1.66^{+0.97}_{-0.23} \times 10^{13g}$	1.14×10^{-05}	$3.47^{+2.02}_{-0.51} \times 10^{27}$	$(1.04 \pm 0.07) \times 10^{29}$	$3.34^{+1.95}_{-0.53}$
			2012 Mar 06.46	$1.46^{+0.89}_{-0.23} \times 10^{13g}$		$2.75^{+1.68}_{-0.43} \times 10^{27}$	$(9.50 \pm 0.70) \times 10^{28}$	$2.89^{+1.78}_{-0.50}$
CO	JCMT	3-2	2011 Dec 30.74	$(9.33 \pm 1.92) \times 10^{13}$	7.49×10^{-07}	$(1.26 \pm 0.26) \times 10^{28}$	$(1.78 \pm 0.07) \times 10^{29}$	7.07 ± 1.49
			2012 Jan 20.84	$(9.12 \pm 2.00) \times 10^{13}$		$(1.06 \pm 0.23) \times 10^{28}$	$(2.37 \pm 0.05) \times 10^{29}$	4.47 ± 0.98
			2012 Jan 22.25	$(9.55 \pm 2.57) \times 10^{13}$		$(1.09 \pm 0.29) \times 10^{28}$	$(1.51 \pm 0.15) \times 10^{29}$	7.22 ± 2.07
			2012 Feb 29.60	$(1.39 \pm 0.35) \times 10^{14}$		$(1.13 \pm 0.28) \times 10^{28}$	$(1.24 \pm 0.10) \times 10^{29}$	9.14 ± 2.41
			2012 Mar 26.29	$(1.16 \pm 0.36) \times 10^{14}$		$(1.01 \pm 0.31) \times 10^{28}$	$(8.63 \pm 0.71) \times 10^{28}$	11.7 ± 3.71
							$(4.60 \pm 0.80) \times 10^{28h}$	22.0 ± 7.73
HCN	JCMT	4-3	2012 Jan 22.82	$(2.63 \pm 0.31) \times 10^{11}$	1.31×10^{-05}	$(3.13 \pm 0.37) \times 10^{25}$	$(1.51 \pm 0.15) \times 10^{29}$	$(2.07 \pm 0.32) \times 10^{-2}$
			2012 Mar 26.34	$(2.90 \pm 0.85) \times 10^{11}$		$(2.57 \pm 0.75) \times 10^{25}$	$(8.63 \pm 0.71) \times 10^{28}$	$(2.98 \pm 0.91) \times 10^{-2}$
							$(4.60 \pm 0.80) \times 10^{28h}$	$(5.59 \pm 1.91) \times 10^{-2}$
			2012 Apr 24.27	$(9.72 \pm 2.43) \times 10^{10}$		$\mathbf{(1.09 \pm 0.32)} \times 10^{24}$	$(3.10 \pm 0.09) \times 10^{28i}$	$(3.52 \pm 1.53) \times 10^{-3}$

[a]The photodissociation rates are from Photo Ionization/Dissociation rates (Huebner et al. 1992)).

[b]Q_{H_2O} from Combi et al. (2013) at comparable dates.

[c]Q_{H_2O} from Bockelée-Morvan et al. (2014).

[d]Corresponds to H$_2$CO as a parent species.

[e]Corresponds to H$_2$CO as an extended source with a parent scale length equal to 4000 $R_h^{1.5}$ km.

[f]Corresponds to H$_2$CO as an extended source with a parent scale length equal to 8000 $R_h^{1.5}$ km.

[g]N_{tot} derived from rotational diagram (see section 4.1).

$^{h}Q_{H_2O}$ from Feaga et al. (2014).

$^{i}Q_{H_2O}$ from Bodewits et al. (2014).

From our SMT and JCMT data we obtain the following average abundance ratios, relative to water: CO: 7.03 ± 1.84 %, HCN: 0.04 ± 0.01 %, o-H_2CO: 0.14 ± 0.03 % as a parent molecule (and 0.28 ± 0.06 % as an extended source), **CS: 0.03 ± 0.01 % (as a parent or daughter molecule)** and CH_3OH: $3.11^{+1.86}_{-0.51}$ %. **The production rate of CS as a parent or daughter molecule are similar due to the short lifetime of the parent specie.**

4.2.1. CO

At mm-submm wavelengths with the IRAM-30m, Biver et al. (2012) found a significant difference in the abundance of CO relative to water between 2011 October 13-21 (5 %) and 2012 February 15-19 (10 %). At submm wavelengths with the JCMT, comet Garradd was observed in four observing runs between 2011 July and 2012 January, and Yang & Drahus (2012) deduced a preliminary CO/H_2O = 7.02 % on 2011 September 23-25. The only CO abundance ratio from observations in the ultraviolet ($\approx$ 20 %), was derived by Feldman et al. (2012) using the Hubble Space Telescope on 2012 January 19. In the infrared Paganini et al. (2012), Villanueva et al. (2012), DiSanti et al. (2014) and Feaga et al. (2014) reported respectively 12.5 %, 10.4 ± 1.5 %, 9.12 ± 1.22 % and 60 ± 1.22 %. (Paganini et al. (2012) acquired spectra of CO with the CRIRES at ESO's Very Large Telescope on 2011 September 18 and 21; Villanueva et al. (2012) detected CO on 2011 September 8 with the CSHELL at IRTF; DiSanti et al. (2014) conducted observations of CO on 2011 October 13 with the NIRSPEC at the Keck II; Feaga et al. (2014) measured CO with the High Resolution Instrument Infrared Spectrometer (HRI-IR) on board the Deep Impact Flyby spacecraft on 2012 March 26 and 2012 April 02). Our value of CO/H_2O (7.03 ± 1.84 %) is consistent with all the values determined at mm-submm and IR except the one reported by Feaga et al. (2014). Indeed, Feaga et al. (2014) show that Garradd exhibited a monotonic increase in CO production throughout the entire apparition (which seems to finally decrease with our observations late March (Figure 3). However, with a decrease in water after perihelion and a increase of CO, Feaga et al. (2014) obtained the highest CO/H_2O ever observed inside 3 AU for any comet ($\sim$60 %). Previous CO-rich comets have had CO/H_2O values ranging from 10-30 %, 4 have ratios >10 %, with only one, C/2008 Q3 (Garradd), reaching $\approx$ 30 % (at R_h = 1.7 AU). **On 2012 March 26, our value for the gas production rate of CO is lower than the one derived by Feaga et al. (2014). By using Q_{H_2O} from Feaga et al. (2014) instead of Combi et al. (2013), we derived a abundance ratio 3 times lower (Table 2).** Feaga et al. (2014) explained the CO-rich composition in some comets by the possible formation of CO in the outer regions of the disk (where the stellar radiation is less intense) or by capture of CO within the water ice mantle. **Due to the different**

abundance ratio bu using Q_{H_2O} from Feaga et al. (2014) or Combi et al. (2013), we used also used Q_{H_2O} from Bockelée-Morvan et al. (2014). We conclude that the difference between the two abundance ratio on 2012 February 18 is negligeable (Table 2).

4.2.2.   HCN

We derived abundance ratio of HCN relative to water between $(3.52 \pm 1.53) \times 10^{-3}$ % and $(6.77 \pm 0.57) \times 10^{-2}$ %. By averaging all the data we obtained a surprising low abundance ratio close to 0.04 ± 0.01 %. Preliminary average ratios have been obtained at mm-submm wavelengths with the IRAM-30m and the JCMT. Both Biver et al. (2012) and Yang & Drahus (2012) derived an average $HCN/H_2O \approx 0.11$ % from data before and after the perihelion. In the infrared Paganini et al. (2012), Villanueva et al. (2012), DiSanti et al. (2014) found abundance ratio between 0.19 ± 0.02 (with the NIRSPEC at the Keck II on 2012 January 8) and 0.37 ± 0.05 % (the CRIRES at ESO's Very Large Telescope on 2011 September). As explain in section 4.2.1, Biver et al. (2012) found a significant difference in the abundance ratio before and after perihelion. Considering the variation with time, the only comparable value after perihelion in given by DiSanti et al. (2014) on 2012 January 8. However, our values with the SMT are lower (2011 December 29, 2012 January 18 - 19) or around (2011 December 28, in the error bars) the typical factor of ≈ 2 between mm-submm and IR measurements (Villanueva et al. 2013). As Feaga et al. (2014), we supposed a seasonal effect or a characteristic of a relatively young comet, but we didn't derive the rotational period due to the lack of time resolution data. We obtained the minimum HCN ratio relative $((3.52 \pm 1.53) \times 10^{-3}$ %) on 2012 April 24. However, we used the Q_{H_2O} at the closest date (2012 April 30) from Bodewits et al. (2014) due to the lack of complimentary observations on 2012 April 24. The low ratio of HCN relative to water can be explained by uncertainties in the water production rate, and possibly the FOV of observations made with different techniques. **To investigate it, we derived the abundance ratio on 2012 March 26 from Combi et al. (2013) (UV) and Feaga et al. (2014) (IR). We found a abundance ratio 2 times higher with the Q_{H_2O} from the IR data (Table 2). However, the difference between the abundance ratio with the Q_{H_2O} from Combi et al. (2013) or Bockelée-Morvan et al. (2014) on 2012 February 18 and 23 is negligeable (Table 2).**

4.2.3. CS

Our derived abundance ratio of CS relative to water (0.03 ± 0.01 %) is in good agreement with the average values derived by Biver et al. (2012) using the IRAM-30m (0.04 %), but by Yang & Drahus (2012) in 2011 September with the JCMT (0.07 %). **As explained in section 4.2, the production rate of CS from the nucleus or from a short-lived species such as CS_2 are similar. We derived mixing ratio on 2012 February 18 and 23 by using Q_{H_2O} from Combi et al. (2013) and Bockelée-Morvan et al. (2014) and found similar results (Table 2).**

4.2.4. H_2CO

The relative abundance of o-H_2CO as an extended source (0.28 ± 0.06 %) is consistent with the average value from Biver et al. (2012), (0.30 %, from submm observations), while its abundance as a parent molecule (0.14 ± 0.03 %) is consistent with that derived by DiSanti et al. (2014) (0.11 ± 0.041 %), obtained on 2011 October 13 with the NIRSPEC at the Keck II. The field of view in the infrared is typically just a few arcseconds, so extended H_2CO sources may not be as obvious in those observations.

4.2.5. Methanol

Our estimate for the abundance ratio of the methanol relative to water, $3.11^{+1.86}_{-0.51}$ %, agrees with those by Bockelée-Morvan et al. (2014), (3.40 ± 0.6%, using the Herschel Space Observatory on 2012 February 22) and DiSanti et al. (2014), (2.14 ± 0.34 %), although all these measures are notably larger than those by Biver et al. (2012) (1.6 %), Yang & Drahus (2012) (1.85 %), and lower than the one by Paganini et al. (2012), (3.90 %).

4.3. Temporal evolution

Our resulting production rates of HCN and CO and others from the literature are plotted with time and heliocentric distance in Figure 3. Observations of comet Garradd spanned 4 months for CO and HCN post perihelion. The temporal evolution of CO and HCN are available in the online journal as supplemental information.

As explained in section 4.2, Combi et al. (2013) and Bodewits et al. (2014) studied in

detail the temporal evolution of water. The water production rate increased as a function of R_h^{-6} then peaked around 50-100 days before the perihelion (Feaga et al. 2014; Bodewits et al. 2014). Q_{H_2O} remained constant for about 100 days, then decreased as a function of R_h^{-4}. Both Combi et al. (2013) and Bodewits et al. (2014) also showed that estimates of the water production rate increased with the observed field of view (FOV). Combi et al. (2013) and Bodewits et al. (2014) thus supported the suggestion of Paganini et al. (2012), Villanueva et al. (2012) and Bockelée-Morvan et al. (2012) that a significant fraction of the water was from an extended source of icy grains, especially pre-perihelion. As suggested by DiSanti et al. (2014) the difference between pre- and post-perihelion might also be due to the seasonal variation in the heating of one or more active region of the nucleus.

In the case of CO, the gas production rate after perihelion remains essentially constant - or perhaps actually increases slightly: the CO production reported by Feaga et al. (2014), 97 days after perihelion, was three times higher than our value obtained 94 days after perihelion. Such behavior for CO, constant or monotonically increasing, has never been observed before. Feaga et al. (2014) suggest that such striking asymmetric activity is either a seasonal effect or a characteristic of a relatively young comet. This could also be a minor outburst event of highly volatile species.

In the case of HCN, the gas production rate increases before perihelion - or perhaps remains constant and decreases after perihelion. The temporal evolution of HCN tends to be similar to the one of water. However, the lack of data does not allow us to study the behavior the gas production between 70 days before perihelion and the perihelion. **Also, the temporal evolution of the gas production rate, of the line profiles or of the shift of the peak line with the SMT shows variation that may be attributed to the rotation of the nucleus.** We tried to obtain the rotational period of the nucleus but the lack of time resolved data made it impossible.

5. Conclusions

We conducted observations of comet C/2009 P1 (Garradd) from 2011 December 28 to 2012 April 04 using the SMT and the JCMT and have reported here detections of HCN, o-H_2CO, CS, CO and CH_3OH. We have derived column densities, production rates, rotational temperature and relative abundances. We concluded that Garradd is normal in CH_3OH, depleted in HCN, o-H_2CO and CS and slightly enriched in CO, which is in good agreement with other studies. Temporal variations in **Garradd's** HCN are similar to water (but with short-term variation), with a decrease after perihelion, while that of CO in the same period shows an unexpected constancy or even increase. The observed short-term variability of HCN
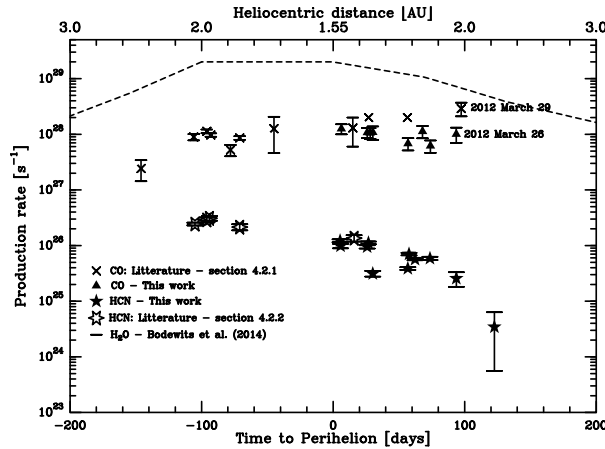
Fig. 3.— Comparison of the evolution of the production rate for HCN and CO around comet Garradd's 2011 perihelion with the H_2O curve. **Bodewits et al. (2014) average data from Combi et al. (2013), Paganini et al. (2012), Bockelée-Morvan et al. (2012), Bockelée-Morvan et al. (2014), DiSanti et al. (2014), Villanueva et al. (2012), Feaga et al. (2014) and Feldman et al. (2012).**

may be due to a seasonal variation or to Garradd's relative youth. These results highlight the importance of studying young comets to better understand their temporal evolution. Long term evolution, complimentary studies, and time resolved data are important for the full analysis and interpretation of cometary data.

REFERENCES

A'Hearn, M. F., Millis, R. C., Schleicher, D. O. et al. 1995, Icarus, 118, 223

Biver, N., Bockelée-Morvan, D., Crovisier, J. et al. 1999, AJ, 118, 1850

Biver, N., Bockelée-Morvan, D., Colom, P. et al. 2012, EM&P, 90, 5

Biver, N., Bockelée-Morvan, D., Lis, D. C. et al. 2012, LPICo, 1667, 6330

Blake, G. A., Masson, C. R., Phillips, T. G. et al. 1986, ApJS, 60, 357

Bockelée-Morvan, D., Crovisier, J. and Colom, P. et al. 1994, A&A, 287, 647

Bockelée-Morvan, D., Biver, N., Swinyard, B. et al. 2012, A&A, 544, L15

Bockelée-Morvan, D., Biver, N., Crovisier, J. 2014, A&A, 562, A5

Bodewits, D., Farnham, T. L., A'Hearn, M. F. et al. 2014, Icarus, 786, 48

Boissier, J., Bockelée-Morvan, D., Groussin, O. et al. 2013, A&A, 557, A88

Combi, M. R., & Fink, U. 1997, ApJ, 484, 879

Combi, M. R., Mäkinen, J. T. T., Bertaux, J.-L. et al. 2013, Icarus, 225, 740

Combi, M. R., Fougere, N., Mäkinen, J. T. T. et al. 2014, ApJL, 788, L7

Cordiner, M. A., Remijan, A. J., Boissier, J. et al. 2013, ApJ, 792, L2

Crovisier, J., Biver, N., Bockelée-Morvan, D. et al. 2009, P&SS, 57, 1162

DiSanti, M. A. & Mumma, M. J. 2008, SSRv, 138, 127

DiSanti, M. A., Villanueva, G. L., Milam, S. N. et al. 2009, Icarus, 203, 589

DiSanti, M. A., Villanueva, G. L., Paganini, L. et al. 2014, Icarus, 228, 167

Drahus, M., Jewitt, D., Guilbert-Lepoutre, A. et al. 2012, ApJ, 756, 80

Ehrenfreund, P. & Charnley, S. B. 2000, ARA&A, 38, 427

Feaga, L. M., A'Hearn, M. F., Farnham, T. L. et al. 2013, AJ, 147, 244

Feldman, P. D., Weaver, H. A., A'Hearn, M. F. et al. 2012, LPICo, 1667, 6165

Gicquel, A., Milam, N. M., Villanueva, G., et al. 2014, ApJ, 794, 1

Horner, J., Evans, N. W., Bailey, M. E., et al. 2003, MNRAS, 343, 1067

Huebner, W. F., Keady, J. J. and Lyon, S. P. 1992, Ap&SS, 195, 1

Jackson, W. M., Butterworth, P. S. and Ballard, D., et al. 1986, ApJ, 304, 515

Levison, H. F. 1996, ASPCS, 107, 173

McNaught, R. H. & Garradd, G. J. 2009, IAU Circ., 9062, 2

Meech, K. J. & Svoren, J. 2004, Comets II, M. C. Festou, H. U. Keller, and H. A. Weaver (eds.), University of Arizona Press, Tucson, 745, 317

Meech, K. J. and Pittichová, J. and Bar-Nun, A. et al. 2009, Icarus, 201, 719

Milam, S. N., Savage, C., Ziurys, L. M., et al. 2004, ApJ, 615, 1054

Milam, S. N., Remijan, A. J., Womack, M., et al. 2006, ApJ, 649, 1169

Morbidelli, A., Levison, H. F., Gomes, R. 2008, The Solar System Beyond Neptune, M. A. Barucci, H. Boehnhardt, D. P. Cruikshank, and A. Morbidelli (eds.), University of Arizona Press, Tucson, 592, 275

Oort, J. H. & Schmidt, M. 1951, Bulletin of the Astronomical Institutes of the Netherlands, 11, 259

Paganini, L., Mumma, M. J., Villanueva, G. L. et al. 2012, APjL, 748, L13

Schloerb, F. P., Irvine, W. M., Friberg, P. et al. 1983, ApJ, 264, 161

Shimonishi, T., Onaka, T. and Kato, D. et al. 2010, A&A, 514, A12

Snyder, L. E., Veal, J. M., Woodney, L. M. and al. 2001, ApJ, 121, 1147

Villanueva, G. L., Mumma, M. J., DiSanti, M. A. et al. 2012, Icarus, 220, 291

Villanueva, G. L., Magee-Sauer, K., Mumma, M. J., et al. 2013, JQSRT 129,158

Yang, B. & Drahus, M. 2012, LPICo, 1667, 6322